SUPPLEMENTARY MATERIAL

Materials and methods

The analysis and sampling of the nummulitic limestone used as building stone in the construction of most important buildings and other architectonic elements such as pavements of the roman city of Dougga was performed in four steps. Firstly, the nummulitic limestones of the buildings were visually recognized and classified in four lithotypes based on macroscopic characteristics like rock texture following Dunham (1962), size of the nummulites, and the presence of terrigenous grains. Secondly, small pieces (up to 4×2 cm) of the four selected lithotypes were sampled from loose and/or fragmented blocks stocked up through the monument in order to proceed with thin section preparation and petrographic study. Thirdly, the limestone succession cropping out in the surroundings of the city was characterized by performing a stratigraphic log traced along the ancient quarries. A systematic sampling of the limestones (24 samples, D4 to D27) for the petrographic study allowed the location of the specific beds or bed sets originally mined in the quarries for each of the four lithotypes. Fourthly, a further sampling of the quarries was performed for subsequent physical-mechanical behaviour and ageing tests. It is important to note that these tests require a large amount of rock material that was not available from the monument.

The petrographic study was performed using an optical polarizing microscope according to the standard test UNE-EN 12407 (2007). Thin sections were stained with alizarin (Lindholm and Finkelman, 1972) in order to distinguish between calcite and dolomite. Depositional limestone fabrics were classified following Dunham (1962).

Petrophysical properties such as pore-size distribution, and water absorption and desorption, compressive strength, abrasion and ageing tests were carried out in order to determine the durability of building materials and to predict their resistance to weathering (Croci & Delgado Rodrigues, 2002; Ghobadi and Babazadeh, 2015; Mamillan, 1991; Zoghlami et al., 2004).

Porous network and pore size distribution was determined using mercury intrusion porosimetry according to the standard ASTM D4404-10 (2010). The samples were analysed with a Micromeritics equipment (AutoPore IV), which allow readings of pore diameters ranging between 0.003 to 360 μm under measuring conditions ranging from (0.003 to 207 MPa). In addition, the porous network configuration has been further characterized by fluorescence microscopy (OFM). Thin section preparations were carried out following the methodology described by Zoghlami & Gómez (2004).

The hydric behaviour of the studied rock was tested on cube-shaped samples (5×5×5 cm) obtained from historical quarries. The following tests have been carried out: (i) Water absorption under vacuum to determine the total open porosity (%) accessible to water and the saturation coefficient (Ws) according to standard test UNE-EN 1936 (2007); (ii) drying test to determine the water retention (Se %) that represents the water content at the end of the drying process and the critical water content Wc (%) (Hammecker & al., 1988), which is indicative of the drying process rate. The Se (%) is calculated with the formula $(M_f - M_0 / M_s - M_0)\times 100$, where M_f is the final mass of the sample at the end of drying process, M_s is the mass of the saturated sample and M_0 is the dry mass of the sample). Experimental conditions were set at 40% relative humidity (RH) and 20°C following the standard test NORMAL 29/88 (1988); (iii) Capillarity water absorption, which let to determine the capillarity absorption coefficient C ($g/(m^2 \cdot s^{0,5})$) indicative of the water suction rate, as it occurs in areas of the buildings in contact with the ground, according to the standard test UNE-EN 1925 (1999); and (iv) compressive strength was tested on prism-shaped samples (5×5×10 cm) according to the standard UNE-EN 1926 (2007). During the performance of both later tests, the samples were oriented parallel to the stratification. Abrasion test was realised according to the standard UNE-EN 14157 (2005). The durability of the rock has been assessed by ice crystallisation ageing test according to the UNE-EN 12371 (2001) standard. Results are expressed calculating the apparent volume variation following the formula $\Delta V = ((Ms_0 - Mh_0) - (Ms_n - Mh_n))\times 100/(Ms_0 - Mh_0)$, where "$Ms_0 - Mh_0$" is the initial apparent volume, "$Ms_n - Mh_n$" the final apparent volume, "Ms_0" the mass of the water-saturated specimen before starting the test, "Mh_0" the hydrostatic mass of the specimen before starting the test, "Ms_n" the mass of the water-saturated specimen at the end of the test, and "Mh_n" the hydrostatic mass of the specimen at the end of the test. The resistance to the action of SO_2 is also assessed according to UNE-EN 13919 (2003), which involve sulphurous acid (H_2SO_3) diluted in water, leaving the solution evaporate inside a closed container where the specimens are stored during 21 days. Two solutions at different concentrations were used, being solution A (25% concentration) and solution B (7.5 % concentration). All realized tests were carried out on three specimens for all lithotypes.

References

ASTM D4404-10, 2010. Standard Test Method for Deterioration of Pore Volume and Pore Volume Distribution of Soil and Rock by Mercury Intrusion Porosimetry, ASTM International Committee, West Conshohocken: PA 19428-2959.

Croci, G., Delgado Rodrigues, J., 2002. Surface and structural stability for the conservation of historic buildings. In Science and Technology of the Environment for Sustainable Protection of Cultural Heritage: EC Advanced Study Course. London: University College London. http://www.ucl.ac.uk/sustainableheritage/ Archive_0906/sustainableheritage/sustainableheritage/learning/asc/delegates/ coursematerials.html.

Ghobadi, M. H., Babazadeh, R., 2015. An investigation on the effect of accelerated weathering on strength and durability of Tertiary sandstones (Qazvin province, Iran). Environ. Earth. Sc. 61, 1327–1336. DOI 10.1007/s12665-010-0451-4.

Hammecker, C., Jeannette D., 1988. Rôle des propriétés physiques dans l'altération de roches carbonatées: Exemple de la façade ouest de Notre-Dame-la-Grande de Poitiers (France). In: VIth International Congress on Deterioration and Conservation of Stone, Ciabach, J. (Ed.), Nicolas Copernicus University, Press Dept.Torum, Poland, pp. 266-275.

Lindholm, RC. et Finkelman, RB., 1972. Calcite staining - semiquantitative determination of ferrous iron. J. Sediment. Res., 42,1, 239-242

Mamillan, M., 1991. Methods for assessing the deterioration of stone monuments. In: N Baer, Baer, N·s, Sabbioni, C. Sors,A.I. (Eds.), Science, Technology and European Cultural Heritage. Proceedings of the European Symposium, Butterworth-Heinemann Publishers, pp 90-99.

Normal 29/88, 1988. Misura delll'indice di asciugamento (Drying Index). CNR-ICR, Roma, 9.

UNE-EN 12371, 2001. Natural stone test methods. Determination of frost resistance.

UNE-EN 12407, 2007. Natural stone test methods. Petrographic examination.

UNE-EN 13919, 2003. Natural stone test methods. Determination of resistance to ageing by the action of SO2 in the presence of moisture.

UNE-EN 14157, 2005. Natural stone test methods. Determination of resistance to abrasion of frictional.

UNE-EN 1925, 1999. Natural stone test methods. Determination of absorption coefficient of water by capillary.

UNE-EN 1926, 2007. Natural stone test methods. Determination of uniaxial compressive strength.

UNE-EN 1936, 2007. Natural stone test methods. Determination of real and apparent density and open and total porosity.

Tables

Table SM1. Petrographic characteristics of the limestones sampled from the stratigraphic log (see Fig. 7 for location).

Samples	Texture classification	Skeletal components	Terrigenous content	Porosity type	Bed thickness	Lithotype
D4 to D6	Grainstone	Nummulites, gastropods, bryozoans, echinoids and red algae	Micritic rock fragments	Intergranular	1-2.5 m	2F, 2G
D7 to D9	Grainstone	Nummulites. Minor discocyclinids and echinoids	Micritic rock fragments and quartz	Moldic	1-1.8 m	L1
D10 to D11	Packstone	Nummulites. Minor gastropods, echinoids and red algae	Quartz	Intergranular and moldic	1-2 m	Not identified
D12 to D15	Grainstone	Gastropods, bryozoans, echinoids	Micritic rock fragments and quartz (<1%)	-	1.5-3 m	Not identified
D16 to D17	Grainstone	Nummulites and echinoids	Partially dissolved micritic grains	Intergranular and dissolution porosity	1-2 m	L3
D18 to D22	Grainstone to rudstone	Ostreids and coarse-sized nummulites	Quartz and lithic fragments	-	1-3 m	L3
D23	Mudstone	-	-	-	0.2 m	Not identified
D24 to D27	Grainstone	Nummulites. Minor gastropods, bryozoans, echinoids and red algae	Quartz	Primary intergranular porosity	2-5 m	2F, 2G

Table SM2. Porometric and hydric parameters of the four studied lithotypes sampled from the historical quarries. Pm = porosity accessible to mercury, Ph = porosity accessible to water; W_s = saturation water content; C = capillarity absorption coefficient; Se = final degree of saturation after drying test regarding to the maximum content of water absorbed under vacuum conditions; W_c = critical water content.

	Porosity parameters (MIP)				Hydric parameters				
Lithotype	**P_m (%)**	**Pore size diameter Mode(nm)**	**Pore size radius Mode (µm)**	**Tortuosity factor**	**P_h (%)**	**Ws (%)**	**C ($g/m^2s^{0.5}$)**	**Se (%)**	**Wc (%)**
L1	2.52 ±0.13	10-20 30-50	0.005-0.010 0.015-0.025	18.96	2.60 ±0.46	1.01 ±0.14	2.80 ±1.69	13.90 ±3.49	0.44 ±0.13
L3	2.02 ±0.25	100-400	0.05-0.20	39.62	2.03 ±0.96	0.77 ±0.39	0.79 ±0.28	22.83 ±5.88	0.37 ±0.16
2F	4.04 ±0.37	100-500	0.05-0.25	10.3	4.10 ±1.85	1.62 ±0.77	3.62 ±1.72	11.02 ±4.49	0.71 ±0.29
2G	3.17 ±0.13	40-100	0.02-0.05	4.96	3.90 ±0.78	1.50 ±0.39	2.86 ±1.70	4.35 ±0.90	0.41 ±0.07

Table SM3. Results of the compressive strength and abrasion test performed on 5×5×5 cm cubic samples. (a) Breaking strength perpendicular to bedding.

Lithotype	[a] Compressive Strength (MPa)	Linear abrasion (mm)
L1	91.40 ±9.41	24.5 ±1.3
L3	71.63 ±7.00	22.8 ±0.8
2F	60.11 ±6.16	22.0 ±2.3
2G	69.40 ±13.64	23.2 ±4.3

Table SM4. Results of the ice crystallization ageing tests performed on 5×5×5 cm cubic samples.

Lithotype	Initial apparent volume (ml)	Final apparent volume (ml)	Volume variation (%)
2F	238.415 ±30.45	236.638 ±30.70	0.767 ±0.27
2G	253.298 ±4.69	251.910 ±4.63	0.548 ±0.03
L1	199.167 ±33.39	197.503 ±33.39	0.852 ±0.18
L3	219.460 ±10.50	218.630 ±10.37	0.377 ±0.07

Table SM5. Results of the resistance to the action of the SO_2 freeze-thaw ageing test for solutions A (25% concentration) and B (7.5 % concentration).

Lithotype	Weight loss (%) Solution A	Weight loss (%) Solution B
L1	0.44 ±0.14	0.22 ±0.04
2F	0.34 ±0.09	0.14 ±0.03
2G	0.31 ±0.05	0.13 ±0.05
L3	0.38 ±0.01	0.13 ±0.01

Table SM6. Petrophysical characteristics of Eocene nummulitic limestones from several Mediterranean countries.

Rock locality	Limestone texture	Porosity (%)	Pore size distribution (µm)	Capillarity C (g/ $m^2 \cdot s^{0.5}$)	Compression strength (MPa)	Freezing decay
Tunisia (this work)	Grainstone	4	0.01-0.5	2.52±1.21	91 ±9.41	Not significant
Spain (Esbert et al., 1989)	Packstone	0.4	0.01-5	0.3±0.003	165 ±15	Not significant
Egypt (Fitzner et al., 2002)	Wackestone to mudstone	12-37	0.1-10 to 1000	-	-	-

Captions of the supplementary figures

Figure S1. Palaeocene to Eocene lithological formations in Tunis (modified from Tlig & al., 2010). The dashed line represents lateral changes in lithological facies.

Figure S2. Google Earth image showing the Roman City of Dougga (left) and the location of the quarries (bottom centre and top right). The red dashed line denotes the trace of the stratigraphic section in Fig. 7.

Figure S3. Photomicrographs of the lithotypes showing most important petrographic characteristics. (A) Lithotype L1 characterized by the partial to complete dissolution of sedimentary rock fragments (arrowed). (B) Lithotype L3 characterized by large nummulites (arrowed). (C) Lithotype 2F showing abundant syntaxial overgrowth cements. (D) Lithotype 2G showing higher proportion and bigger nummulites than lithotype 2F.

Figure S4. Field images of the quarries located in the surroundings of Dougga. (A) Field panorama showing the lower quarry (see Fig. 1 for location). (B) Detail of A (square) showing the bedding in the front part of the quarry and the trace of the stratigraphic log (red dashed line). Note the metre-scale thickness of the bedding in the bottom and top of the front. (C) Base of the lower quarry showing shaped metre-scale stone blocks ready to use. The origin of these ashlars is unknown, but they are most probably post-Roman. (D) Top of the lower quarry, showing marks of the extraction. Note the metre-scale thickness of the bedding. (E) Top beds of the lower quarry, showing marks of the extraction. The size and the lithotype of the rock suggest that the extracted blocks were used as columns. The surface dipping towards the right corresponds to the bedding. (F) Detail of E showing well-preserved lines of wedge-marks from splitting (arrow), presumably Roman in origin. (G) Panoramic view of the upper quarry.

Figure S5. Stratigraphic log of the lithological succession cropping out in the surroundings of Dougga, showing the bedding characteristics of the nummulitic limestone, and the location of the samples (D-) and major quarries (see Fig. 1 for location). Pkst = packstone, Grst = grainstone, Wckst = wackstone.

Figure S6. Pore size distribution of the four lithotypes showing smaller mean pore diameter in L1 (10–20 nm), medium in 2G and 2F (40–100 nm and 100–500 nm, respectively), and bigger in L3 (100–400 nm).

Figure S7. OFM images under fluorescence light showing the porous network (green colour) of the limestones. Most common pore types are vugs (A) and fissures (B).

Figure S1

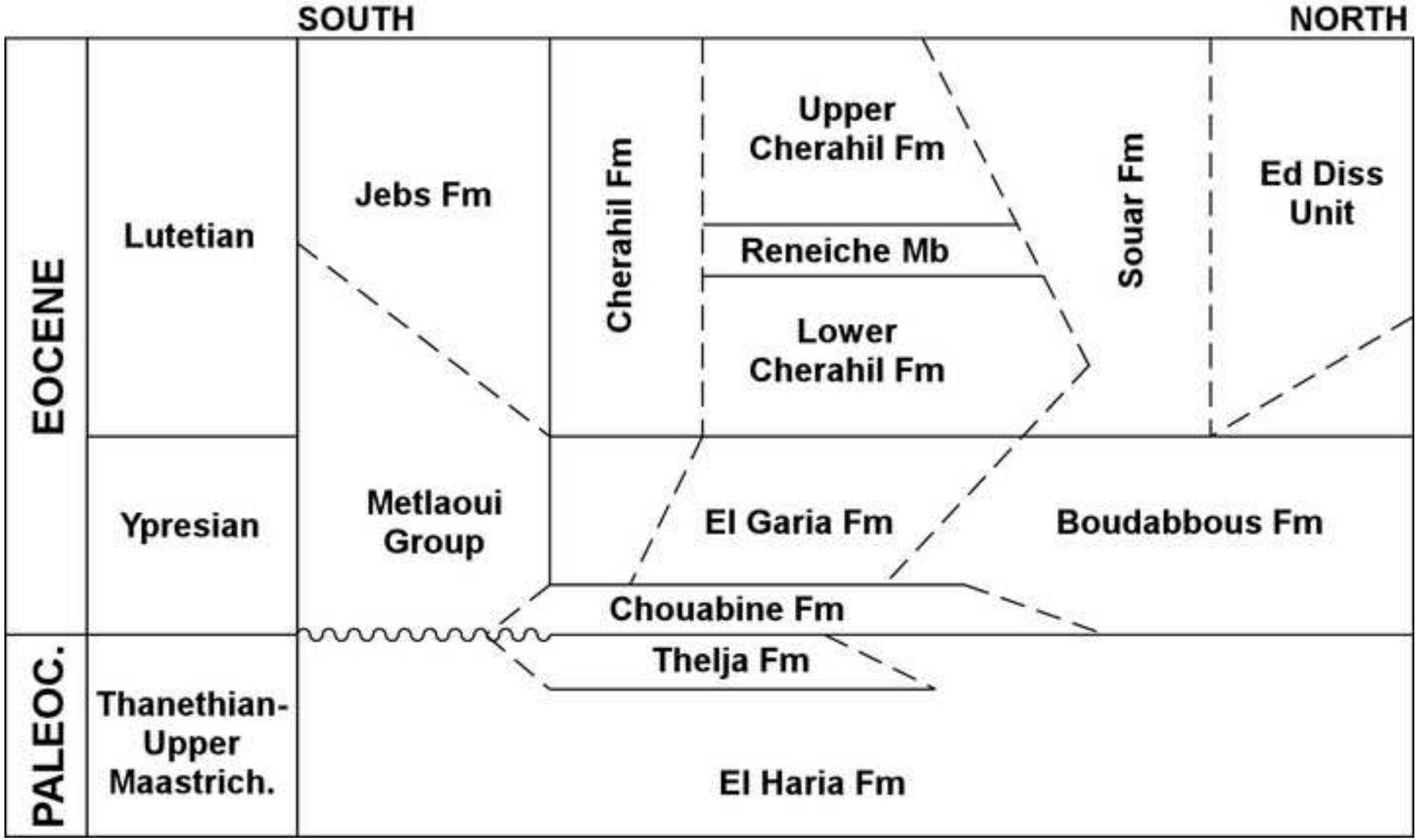
SOUTH
NORTH
EOCENE
PALEOC.
Lutetian
Ypresian
Thanethian-
Upper
Maastrich.
Jebs Fm
Metlaoui
Group
Cherahil Fm
Upper
Cherahil Fm
Reneiche Mb
Lower
Cherahil Fm
Souar Fm
Ed Diss
Unit
El Garia Fm
Boudabbous Fm
Chouabine Fm
Thelja Fm
El Haria Fm

Figure S2

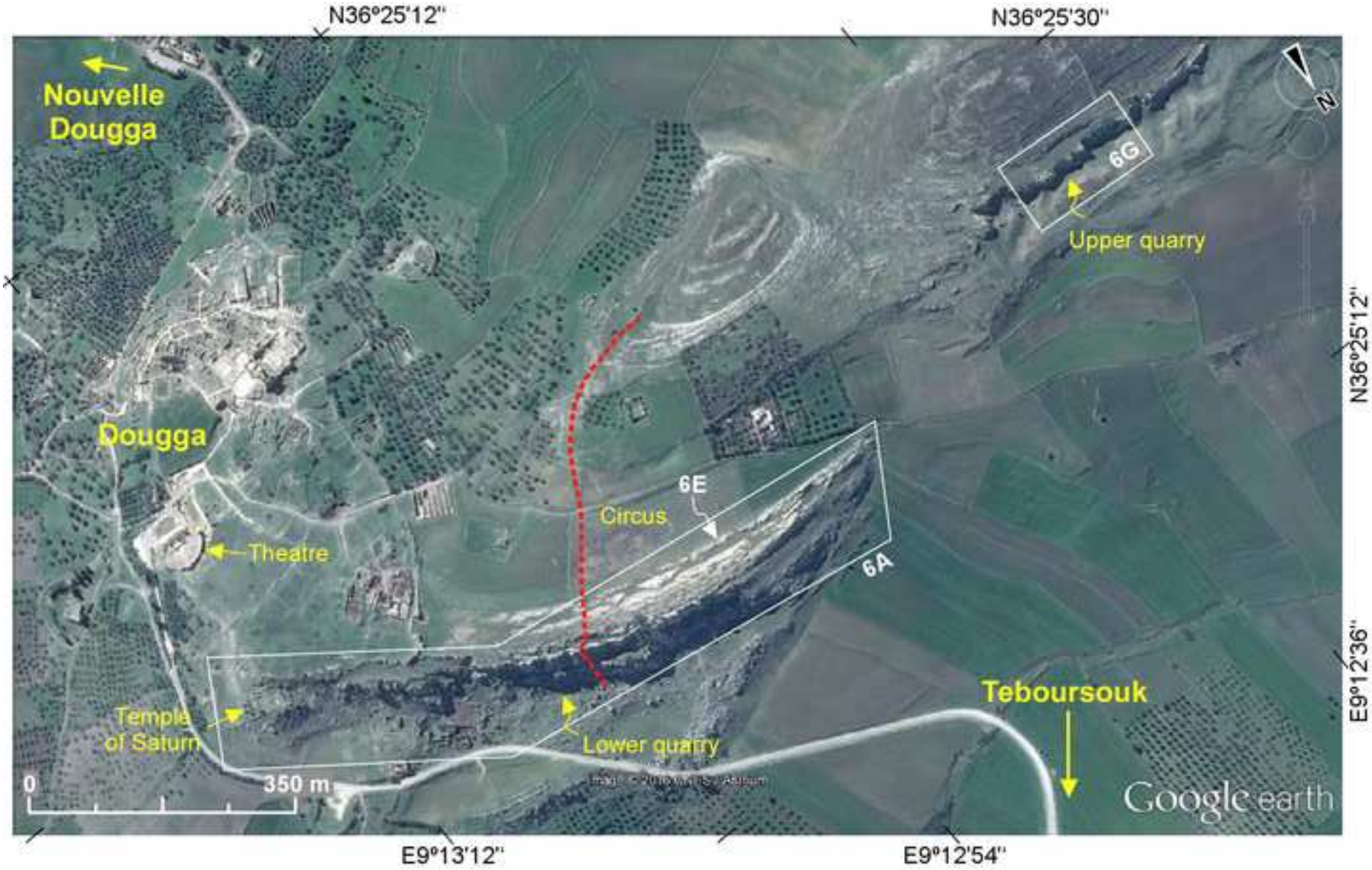
N36°25'12"
N36°25'30"
Nouvelle Dougga
Dougga
Theatre
Circus
6E
6A
6G
Upper quarry
Temple of Saturn
Lower quarry
Teboursouk
0
350 m
N
N36°25'12"
E9°12'36"
E9°13'12"
E9°12'54"
Google earth

Figure S3

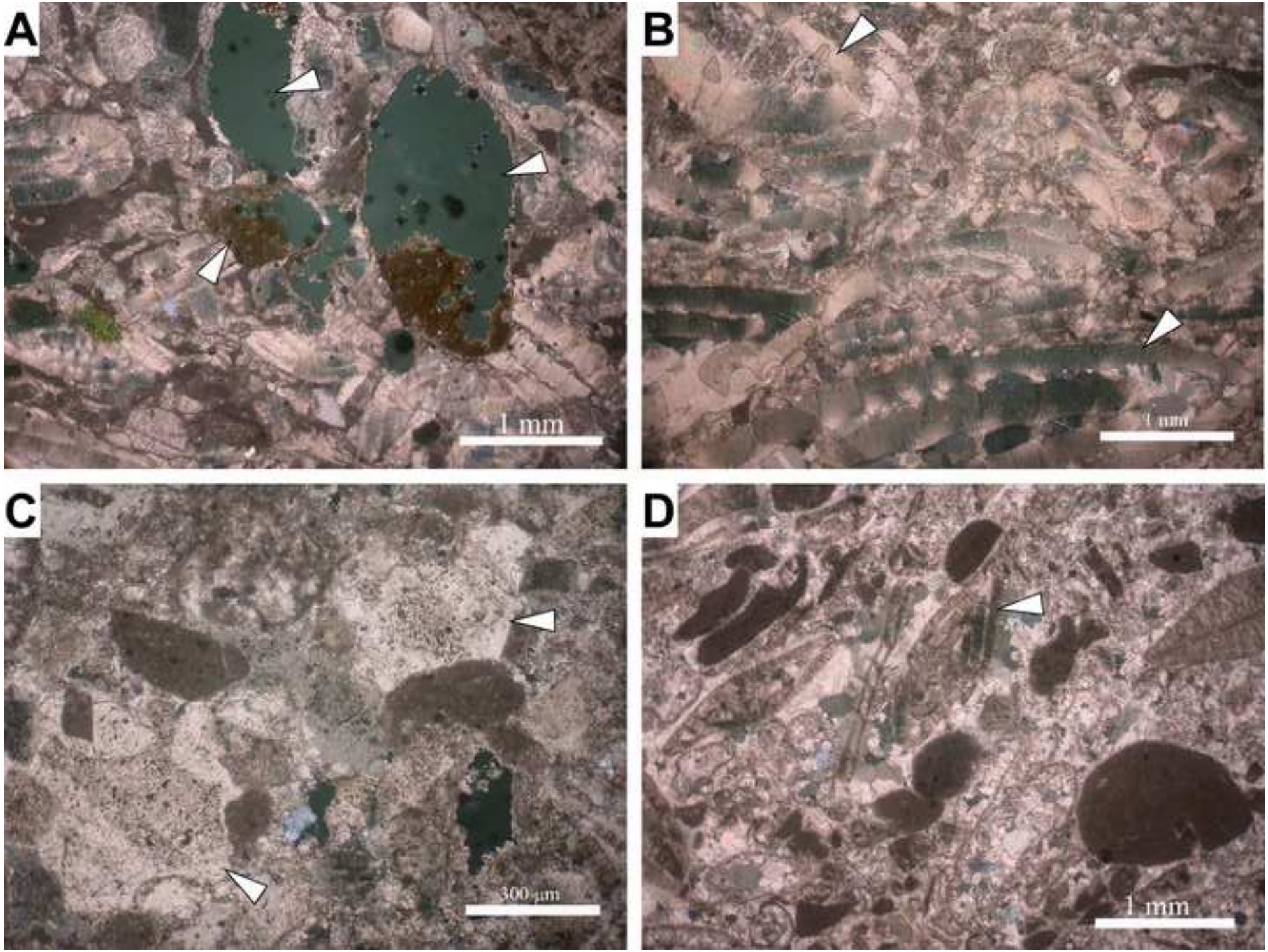

Figure S4

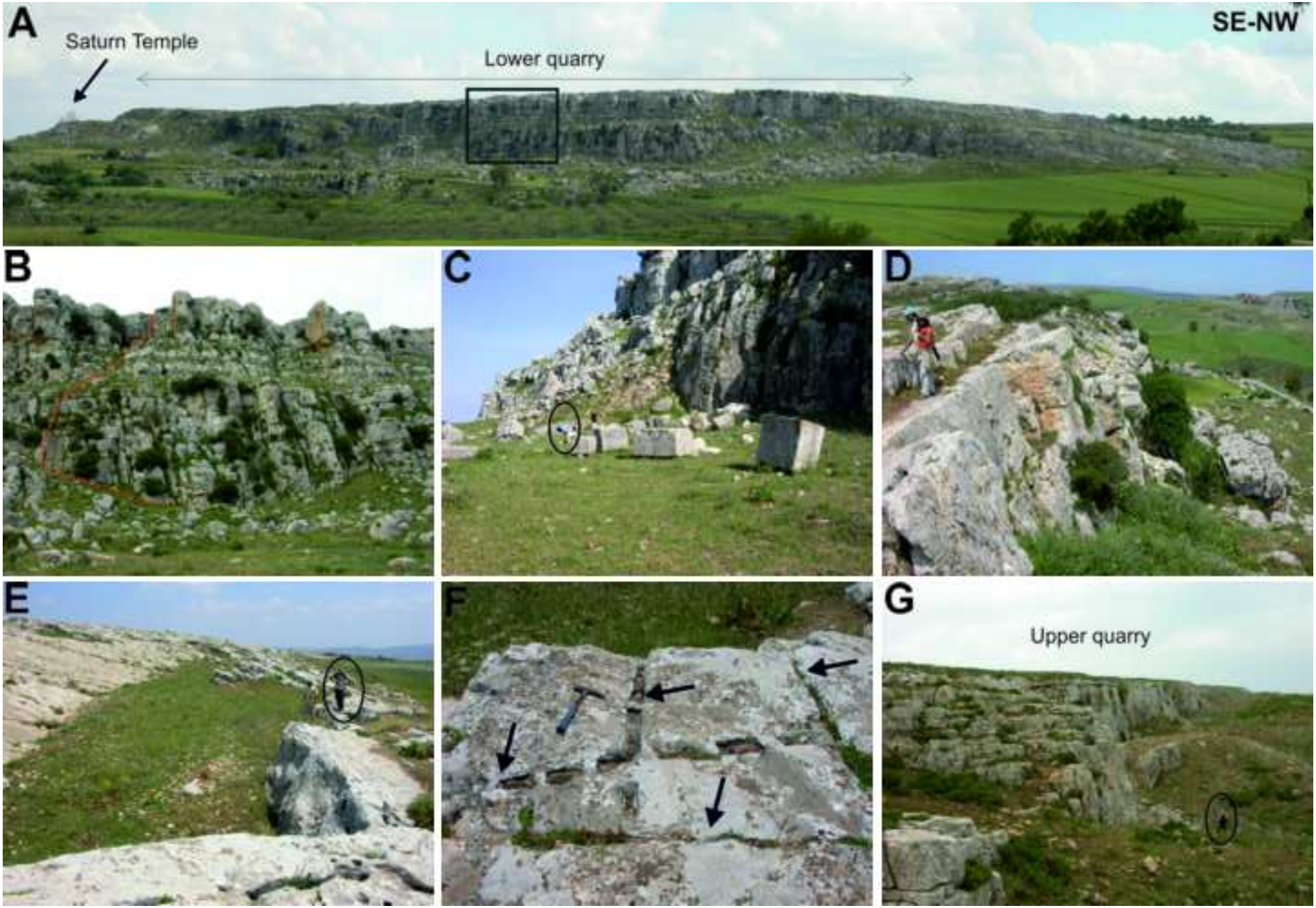

Figure S5

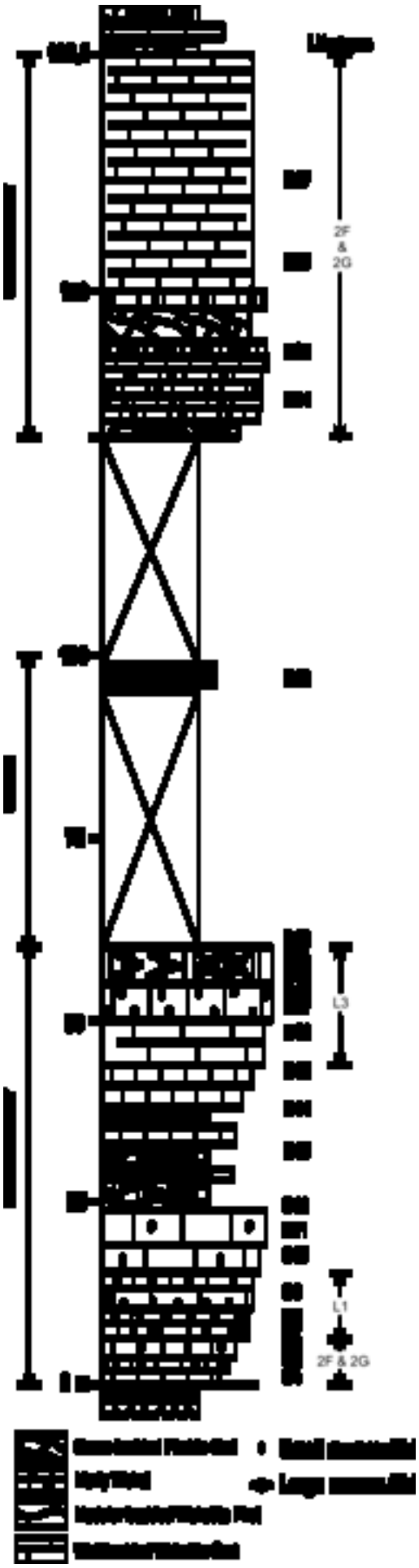

Figure S6

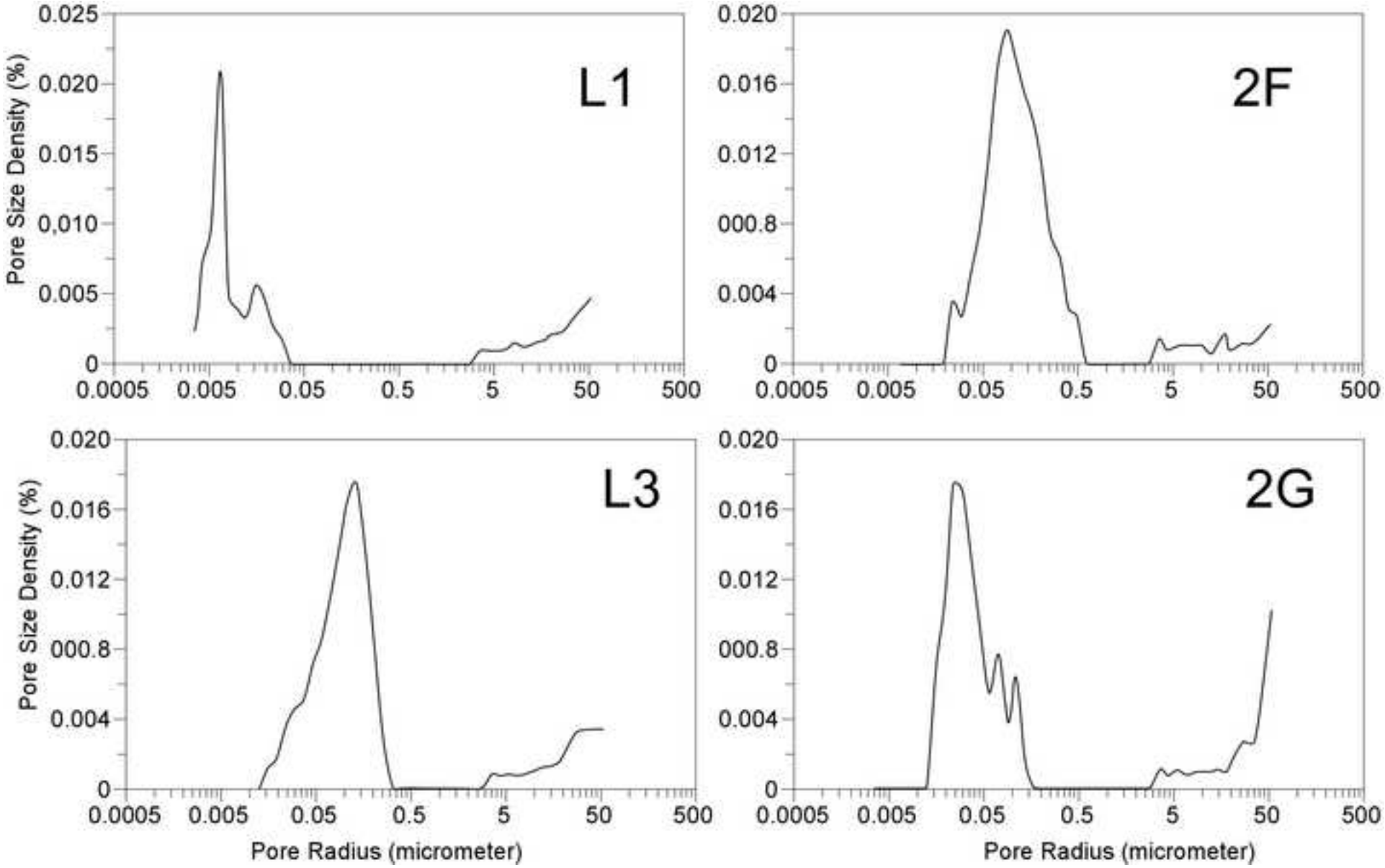
L1
2F
L3
2G
Pore Size Density (%)
Pore Radius (micrometer)
0.025
0.020
0.015
0,010
0.005
0
0.016
0.012
000.8
0.004
0.0005
0.005
0.05
0.5
5
50
500

Figure S7